Supporting Information of

Selective glycerol to lactic acid conversion via a tandem effect between platinum and metal oxides with abundant acid groups

Hui Luo,[1,2†] Mianle Xu,[3†] Sihang Liu,[3] Giulia Tarantino,[1] Hanzhi Ye,[1] Hossein Yadegari,[4] Alain Y. Li,[1] Ceri Hammond,[1] Georg Kastlunger,[3*] Ifan E. L. Stephens,[4*] Maria-Magdalena Titirici[1*]*

Table of Contents

1. Catalyst Surface Characterization

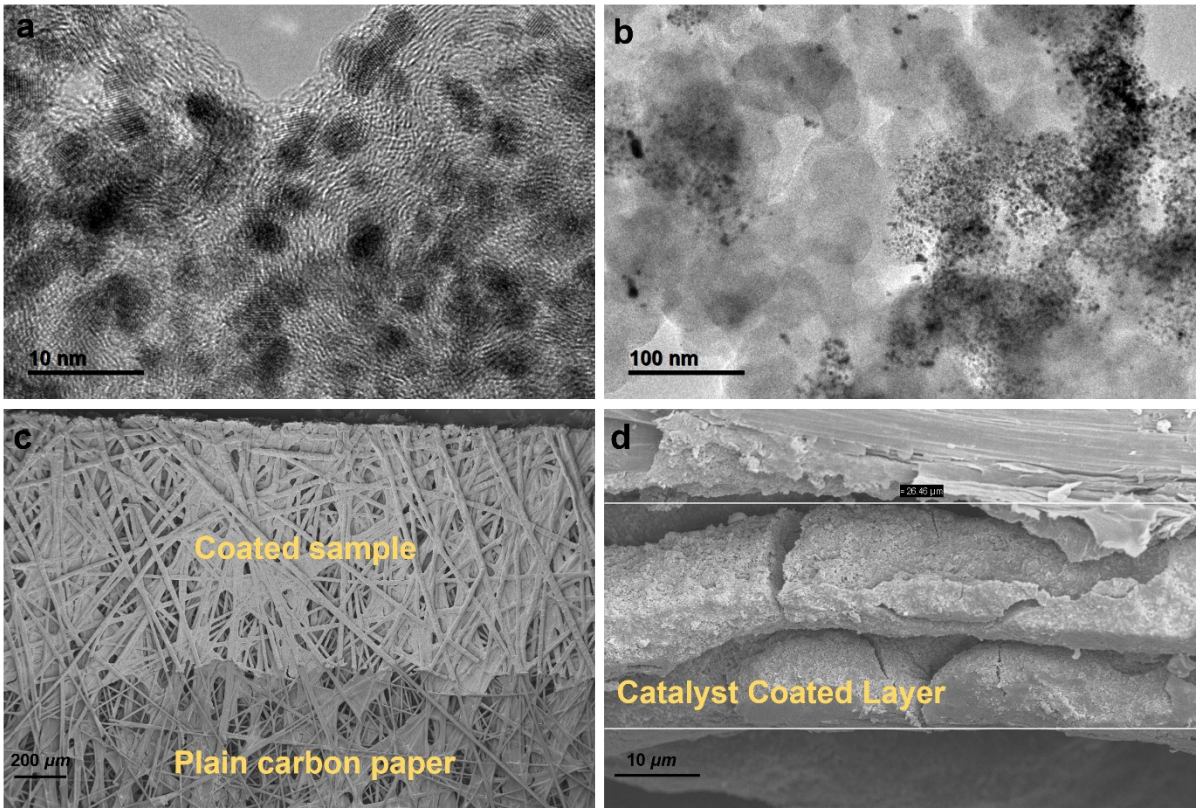

Figure S1. Pt/C catalyst and electrode morphology. a and b. The morphology of the Pt/C catalyst was first investigated with transmission electron microscopy (TEM). The Pt/C nanoparticles have a diameter of 3-5 nm, and in close contact with the carbon black substrate. c and d. are the scanning electron microscopy (SEM) images of the Pt/C coated carbon paper electrode. After coating, the electrode colour changed slightly, and the catalyst coated layer is approximately 26.5 μm in thickness.

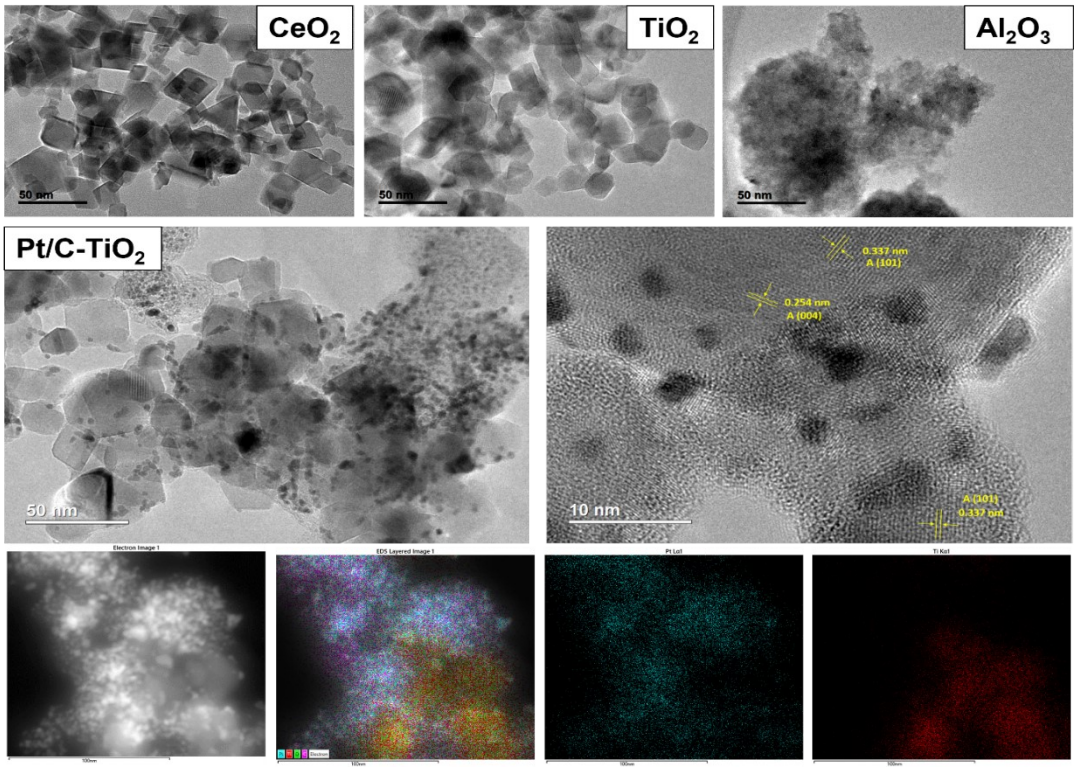

Figure S2. Pt/C-MO_x multicomponent catalyst morphology

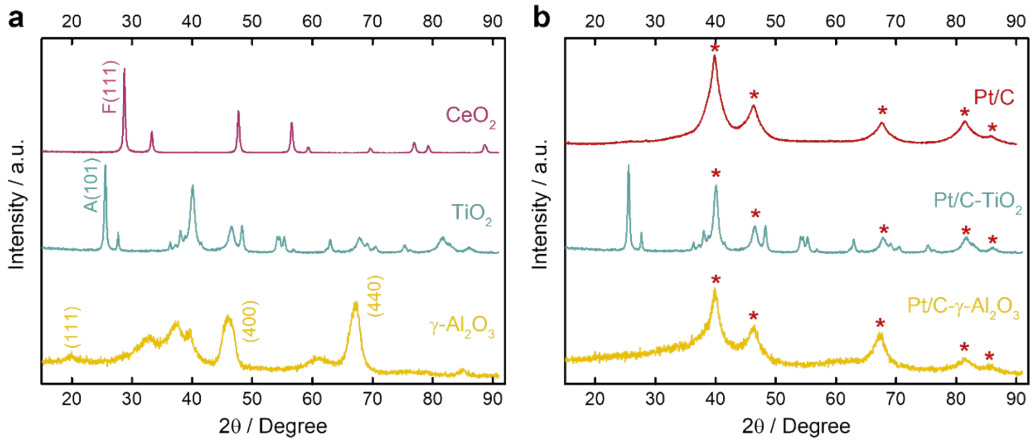

*Figure S3. Pt/C-MO_x multicomponent catalysts structure. a: XRD for three different kinds of metal oxides; b: XRD for Pt/C, Pt/C-TiO_2, Pt/C- γ-Al_2O_3. The diffraction peaks labelled with * are from Pt.*

2. Free Energy Diagrams (FED) on Pt(111)

a) Free energy diagram at 0V vs RHE

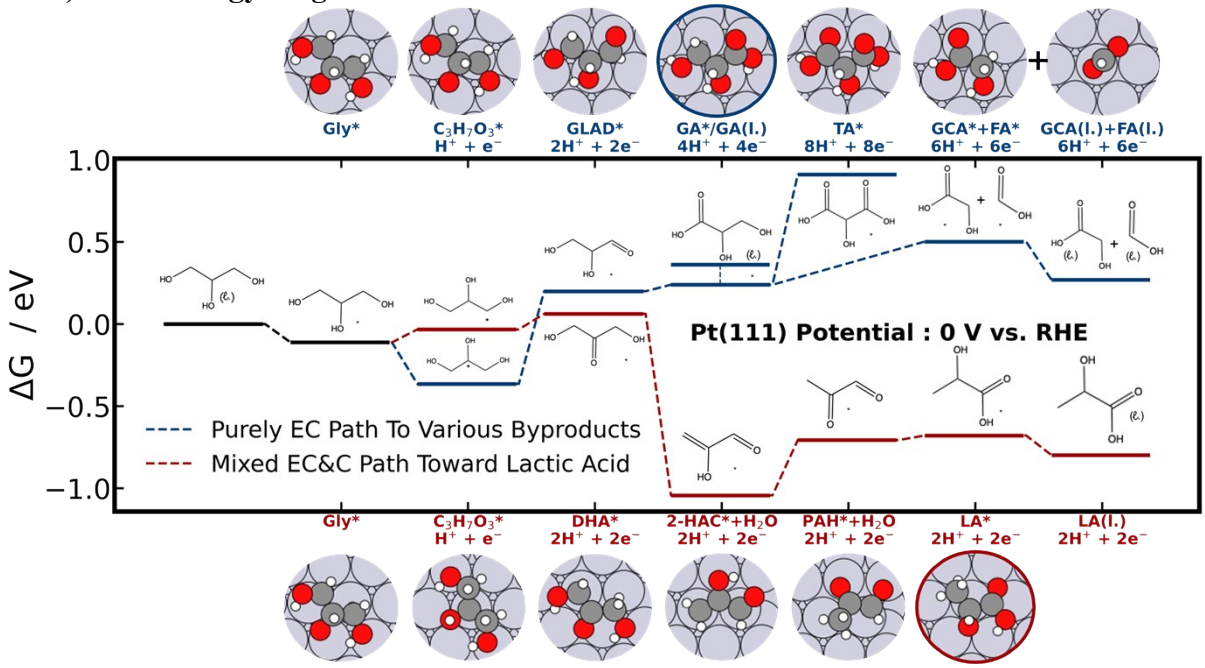

Figure S4. Free energy diagram of glycerol electro-oxidation on Pt(111) at 0 V vs. RHE. Note that, that to the FED at 0.5V vs RHE shown in figure 4, the electrochemical pathway shown in blue changes with the applied potential, while the non-electrochemical steps following DHA are unaffected by it.

b) Complete electrochemical pathway

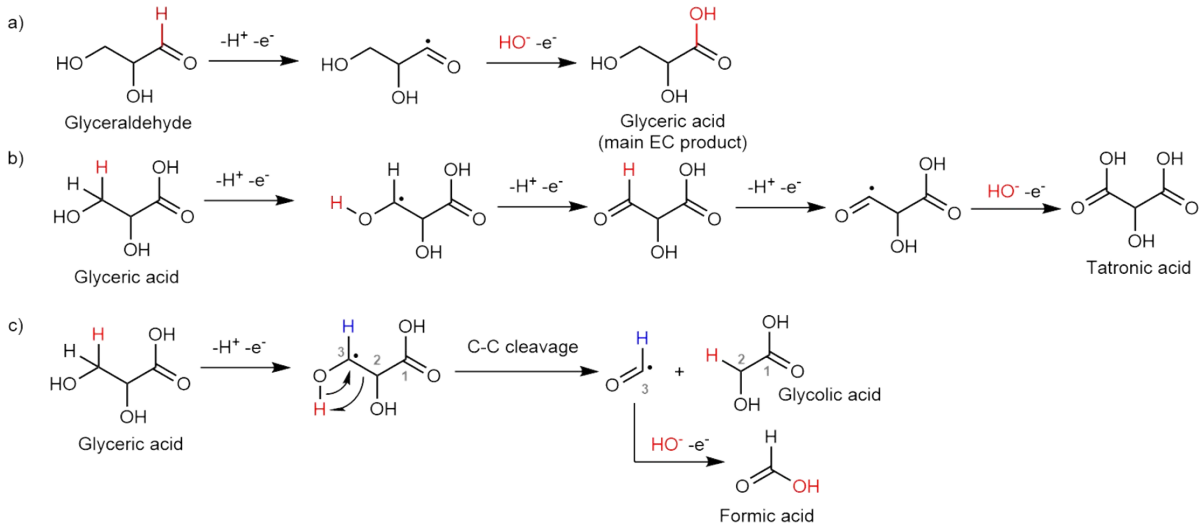

Figure S5: The elementary steps of the full electrochemical pathway: a: the mechanism from glyceraldehyde to glyceric acid; b: the continuous proton-electron transfer mechanism from glyceric acid to tartronic acid; c: the possible mechanism of C-C splitting; glyceric acid splits into formic acid and glycolic acid.

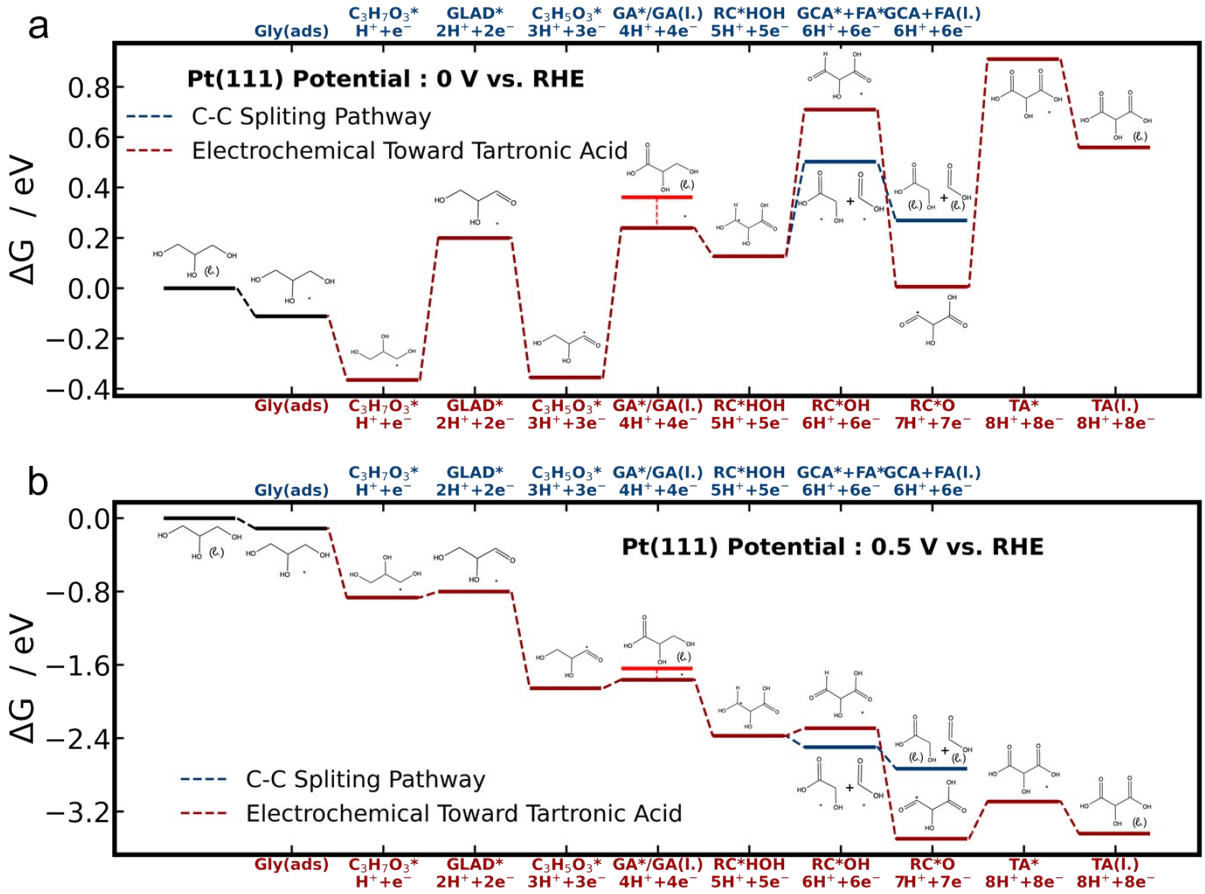

Figure S6 The free energy diagram of the full electrochemical pathway on Pt(111) at a: 0V and b: 0.5V vs RHE. The bright red bar in the middle is the desorption of glyceric acid. The dark red line is the elementary step toward tartronic acid, the blue line represents the steps of C-C splitting.

3. Electrolysis Data

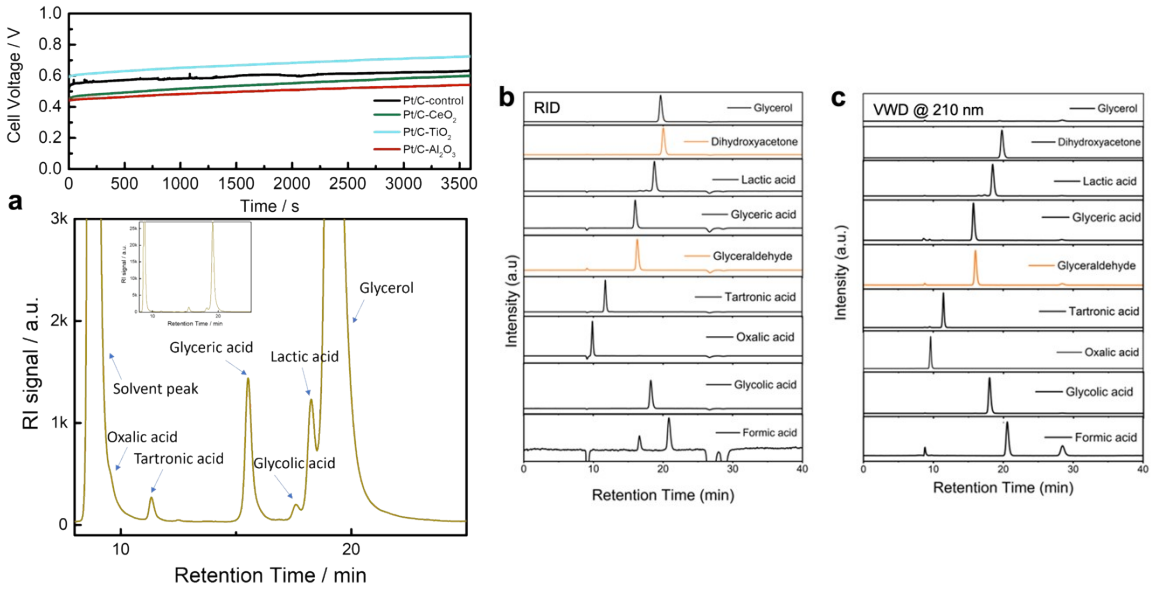

Figure S7. a. (Top) The corresponding electrolysis data Cell Voltage vs. time on Pt/C and Pt/C with different metal oxides. (Bottom) HPLC chromatograph compound assignment; b. single compound calibration using RID detector; c. the corresponding single compound calibration with VWD at 210 nm wavelength. The glycerol peak is largely suppressed, but the rest of the compound remain comparable.

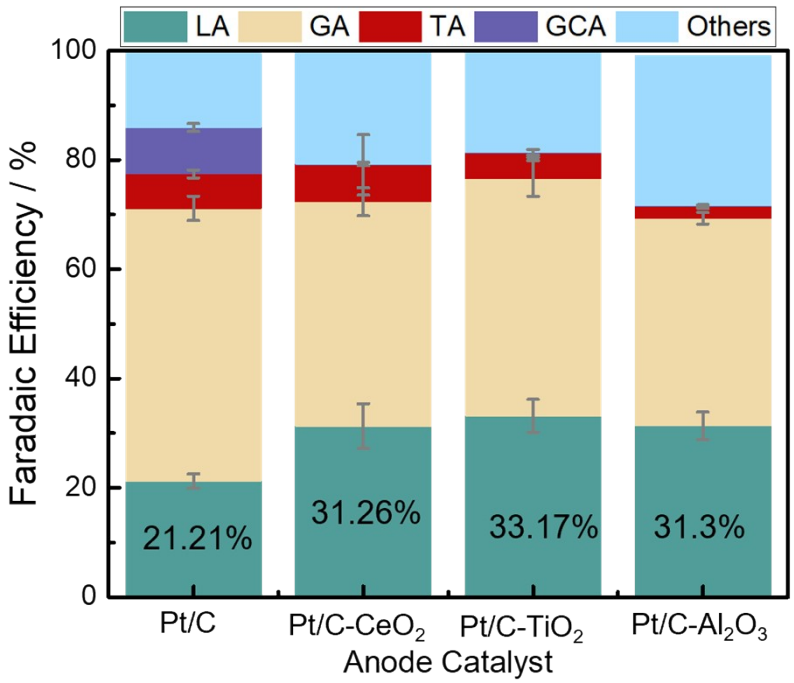

Figure S8. The Faradaic Efficiency % for Pt/C-MOx and Pt/C control. Values are averaged from at least three independent measurements. Current density: 20 mA cm^{-2}. Electrolysis duration: 1 h.

Table S1 Summary of literature reports for electrochemical glycerol conversion to lactic acid. The LA / % values reported here is the liquid product distribution towards lactic acid defined as: mole of lactic acid/mole of total liquid products detected × 100%.

Ref	Catalyst	$[C]_{glycerol}$/M	$[C]_{base}$/M	Current density (mA cm^{-2})	LA / %	Cell type
4	Co-DPPE	0.25	1M	1.3	33.4	Static half-cell
				1.8	38.6	
				4.4	34.7	
				8.8	34	
				13.3	29.5	
				22.1	21.2	
				44.2	9.78	
5	Pt_3Au_7@Ag	0.5	0.5	0.25	17	Static half-cell
6	Pt-CBAC	0.3	0	60.6	20.7	Static half-cell
7	Pt-CC	4	2	60	28	MEA
				120	30	
				180	34	
8	Ni_xBi_{1-x}	0.5	2	15	33.8	Static half-cell
9	Planar Au	0.1	1	1	29.45	Static half-cell
10	Au NWs	0.3	3	387	80	Static half-cell
11	$Au/Ni(OH)_2$	0.3	3M	317	77	Static half-cell
				43.3	65	MEA
12	AuPt (15% Pt_{Surf})	0.5	1	1.89	72.5	Static half-cell
13	Au	0.5	3	331.3	44	Static half-cell
	Au/CeO_{2-x}	0.5	3	693	81	Static half-cell
14	Pt/C-Zeolite	1	1	20	57.3	MEA
15	hp-PtAu/NF	0.5	1	921.5	70	Static half-cell
This work	$Pt/C-Al_2O_3$	1	1	20	64	MEA

4. Surface Acidity Characterisation

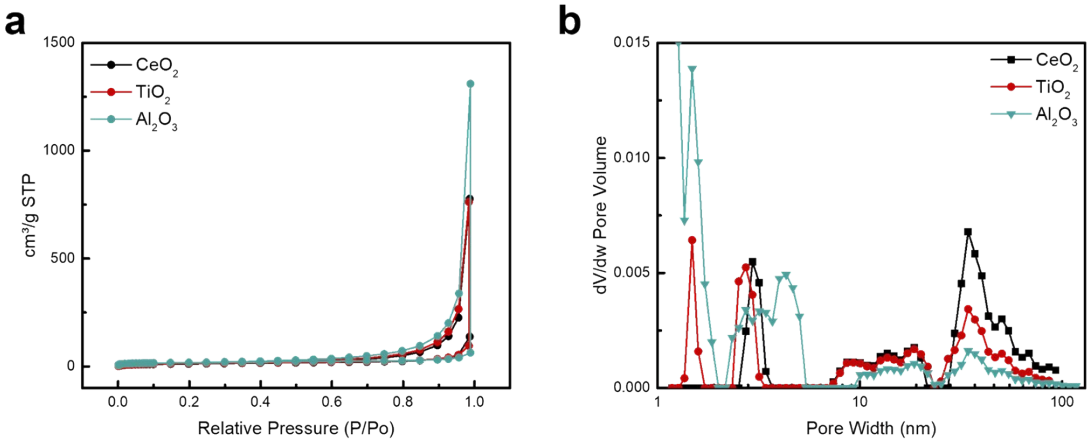

Figure S9. BET isotherm (a) and pore size distribution profile (b) of the MO_x additives.

Table S2. BET specific area and surface acidic sites of the different additives.

Catalysts additives	BET (m^2 g^{-1})	Surface acidic sites (mmol g^{-1})
Carbon black	62	0.012
CeO_2	45	0.195
TiO_2	51	0.252
Al_2O_3	63	0.490

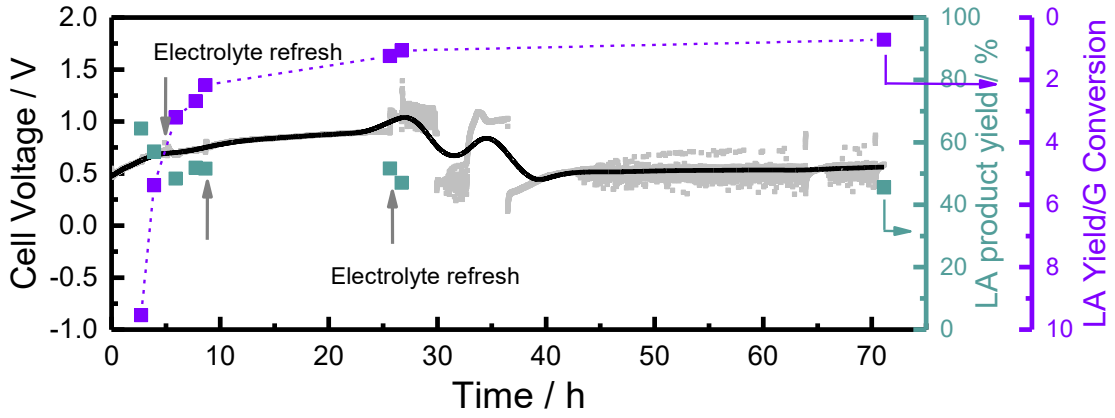

Fig S10. Extended stability measurement of the glycerol electrolysis process. Current density: 20 mA cm^{-2}. Temperature: 60 °C. Anolyte: 1 M Glycerol/1 M NaOH; catholyte: 1 M NaOH. The lactic acid product yield is defined as Product Yield % = $\frac{produced\ lactic\ acid\ in\ mole}{consumed\ glycerol\ in\ mole} \times 100\%$, and the LA yield/G Conversion is defined as the lactic acid product yield in percentage / glycerol conversion in percentage.

During stability test, the electrolyte was refreshed at 5, 9 and 25 h. Such procedures have caused disturbance to the electrolysis profile, as shown in the noisy data points around these time stamps. We have therefore simulated the actual data with a smooth function, as shown with the black line. After the 3rd electrolyte refresh, the cell voltage temporarily rose above 1 V, where carbon corrosion might take place. The big perturbation and voltage jump immediately after the 3rd electrolyte refresh was due to the interference with the electrolyser set-up which caused the system became unstable. After a few adjustments, the voltage went back to normal (around 0.5 V) at 37h, until after 45h when the voltage started to raise up again. At this point it is likely the Pt was getting poisoned by surface adsorbed intermediates, and we have thus applied pulsing to mitigate the poisoning effect. As the glycerol continued to be consumed, the lactic acid product yield drops from 64.4 % to 45.5 % after 72 h test, but a plot of lactic acid product yield / glycerol conversion rate as displayed in purple in Figure 10 demonstrates the effectiveness of the process.

5. Computational details

a. DFT Parameters and Description

All DFT calculation have been conducted with the Vienna Ab initio simulation package (VASP)[2] combined with the projector-augmented-wave (PAW)[3] formalism for treating core electrons. The plane wave energy cutoff of valence electrons were set to 500eV and Methfessel-Paxton smearing with a width of 0.2 eV was used. We employed the revised Perdew−Burke−Ernzerhof (RPBE)[4]

functional to describe the exchange and correlation energies. For the dispersion contributions, the Grimme D3-functional[5] was applied in all the calculations.[6]
A kpoint sampling[7] of 3x3x1 was applied for the metal oxides CeO_2(111) and γ-Al_2O_3(111), and a 3x4x1-mesh was used for Pt(111) and Anatase-TiO_2(101) surfaces. The surface structures are shown in **Fig. S12**.
To evaluate the active sites and different molecule orientations at the surface, for the stable molecules, the adsorption configurations were sampled from 5 individual calculations by different sites and orientations. In some cases, due to the bad initial guess of the structures, the C3 chain spontaneously split during the DFT relaxation. We ignored such relaxation outcomes when calculating the adsorption energy. The adsorption and formation energies reported throughout correspond to the most stable geometries, resulting from this sampling procedure. All relevant adsorption data is provided in the repository noted in the Data & Availability section of the main article. For the metal oxide calculations, we initially compared DFT and DFT+ U on Anatase-TiO_2(101) surface applying a U-value of 2eV for Ti.[8] For the glycerol adsorption, we found that with or without U correction, the adsorption energy results are –1.03eV and -0.98eV, respectively. Thus, we refrained from using a Hubbard-U correction to calculate all the adsorption energy on metal oxides surface.
For the free energy calculations, the zero-point energy, head capacities and entropy corrections were calculated from the ab-initio vibrational frequencies from VASP (IBRION=5). For the surface adsorbates, we used the Harmonic limit approximation. For the molecules in gas phase, we used the ideal gas approximation to calculate the vibrational contributions to the free energy.[9] The temperature used in free energy calculations was set as experimental temperature (60°C, ~333K). The computational hydrogen electrode (CHE)[10] model was applied to account for the effect of the electrode potential in the electron transfer steps in the free energy diagram.

b. Adsorbates, Key Intermediates, Reference States

We calculated the adsorption energies of all (meta)stable molecules, key intermediates, and the intermediates of Proton-Couple Electron Transfers (PCET) on Pt (111). For the high band gap of metal oxides, the electron transfer steps are not viable due to the lack of electronic conductance, so we only calculated the key intermediates in the dehydration steps towards lactic acid. The reference states in our calculations are (liquid) glycerol ($C_3H_8O_3$), hydrogen gas (H_2), and water (H_2O). All the reference states have been calculated in gas phase, and to access the liquid phase chemical potential of glycerol and water, we used the saturated vapor pressure as listed in subsection f. For hydrogen gas, we used 1 atm as reference pressure. **Fig. S11** shows the molecules and intermediates we considered and calculated in this paper.

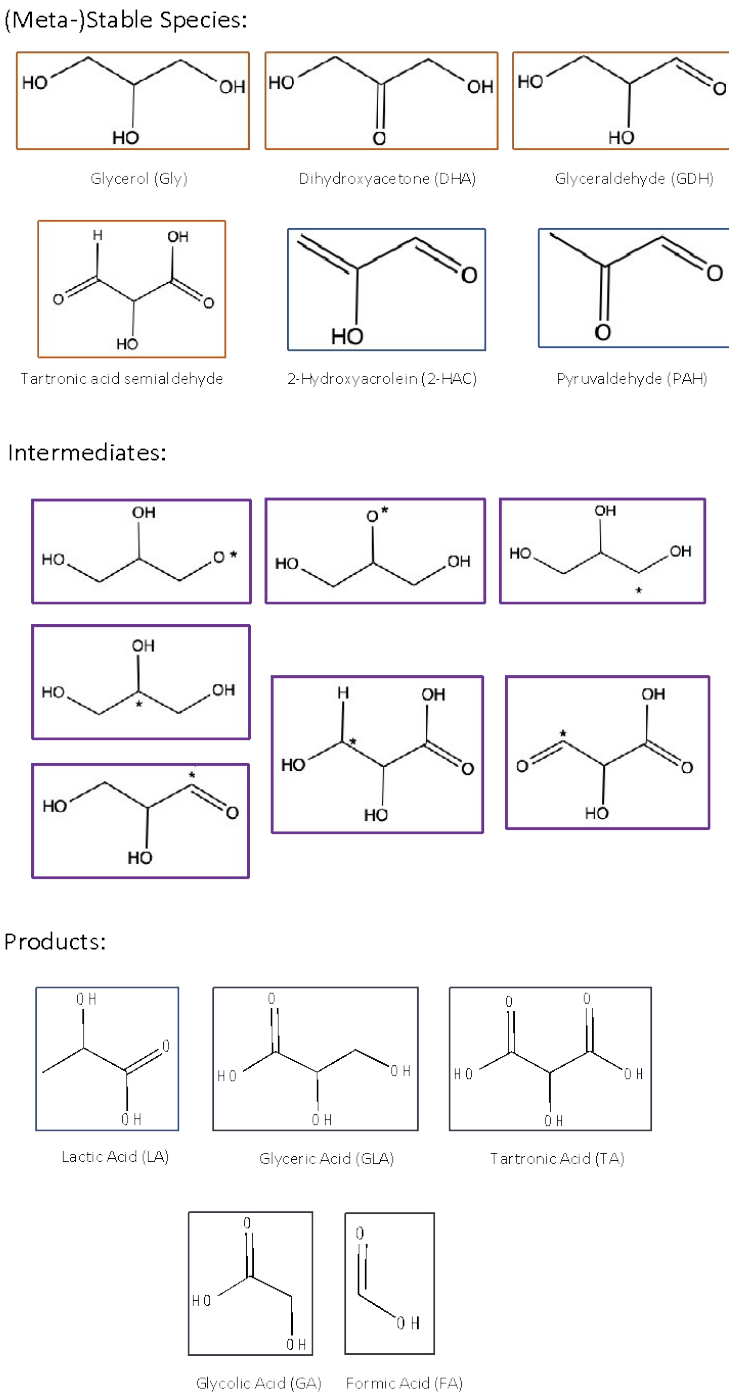

*Figure S11 The adsorbates considered in our DFT calculations. In the first block, we show the (Meta-)Stable species, which are the closed shell organic compounds that exist on the surface (orange rectangles), and the precursors of Lactic acid (blue rectangle). The second block (purple rectangles) shows all the possible intermediates of the PCET steps, with the symbol * marking the atom bound to the surface. The third block shows the products of glycerol oxidation which result from a combination of electrochemical and –hydrolysis steps (in blue rectangle) and continuous electro-oxidation (in gray rectangle).*

c. DFT Structures: Relaxed Adsorption Structures

In our surface modelling, we built our surface slabs of CeO_2 and TiO_2 based on the XRD result of the catalyst (see **Fig. S2** and **Fig. S3**). The lattice parameters of each metal/metal oxides were optimized, and their final values are summarized in Table S3. We built 4 layer 4x4 Pt

(111), 4 layer 4x2 Anatase-TiO_2(101) , 3 layer CeO_2 (111) , and 4 layers γ-Al_2O_3 (111). For all slabs the bottom 2 layers were frozen. 15Å of vacuum has been applied between repeated slabs. The adsorbates were placed on the unfixed side of the slab surface and the initial distance between the first layer atom and the adsorbate was set to 2.5-3.

For modelling amorphous γ-Al_2O_3, we used the bulk phase structure from Ref.[1] to build the γ-Al_2O_3 (111) surface. Initially, we built the (400), (440) and (111) surface facets of the crystal. Upon initial relaxation the (400) and (440)-heavily reconstructed, while the (111)-surface remained stable. Thus, we chose the latter for our simulations.

Fig. S12 shows the clean surface structure of the catalysts used in this paper.

Table S3. The calculated lattice parameters from DFT

Compositions	**Lattice system**	**Lattice parameters (Å)**
Pt	**Cubic**	a=3.93952 Å
Anatase-TiO_2	**Tetragonal**	a=3.80845 Å c=9.47269 Å
CeO_2	**Cubic**	a=5.4249 Å
γ-Al_2O_3	**Triclinic**	a=9.98658 Å b=9.68584 Å c=9.77964 Å alpha=110.842° beta=108.48° gamma=108.074°

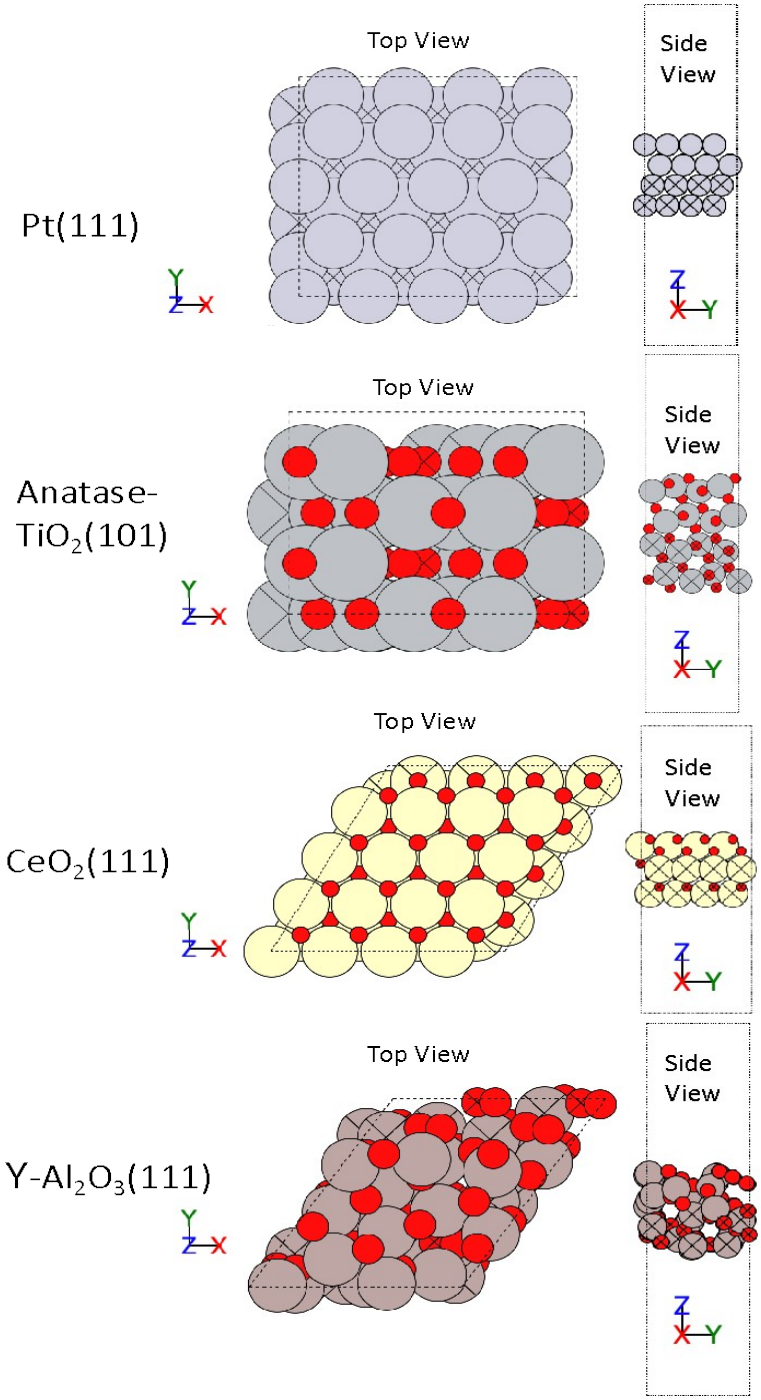

Figure S12 The clean surface structures of Pt(111), Anatase-TiO_2(101), CeO_2(111) and γ-Al2O3. These surfaces were applied to calculate the various adsorption and formation energies. Color codes for atoms: grey – platinum, silver –titanium, yellow – cerium, pink – aluminium, red – oxygen.

Fig. S13 shows the relaxed adsorption structures on all studied catalysts. 5 different active sites and molecular orientations were sampled to identify the adsorption structures. The relaxed structures shown here are the most stable ones of each sampling. All the structures and adsorption free energy are in our database, see Data & Code Availability section in the main article.

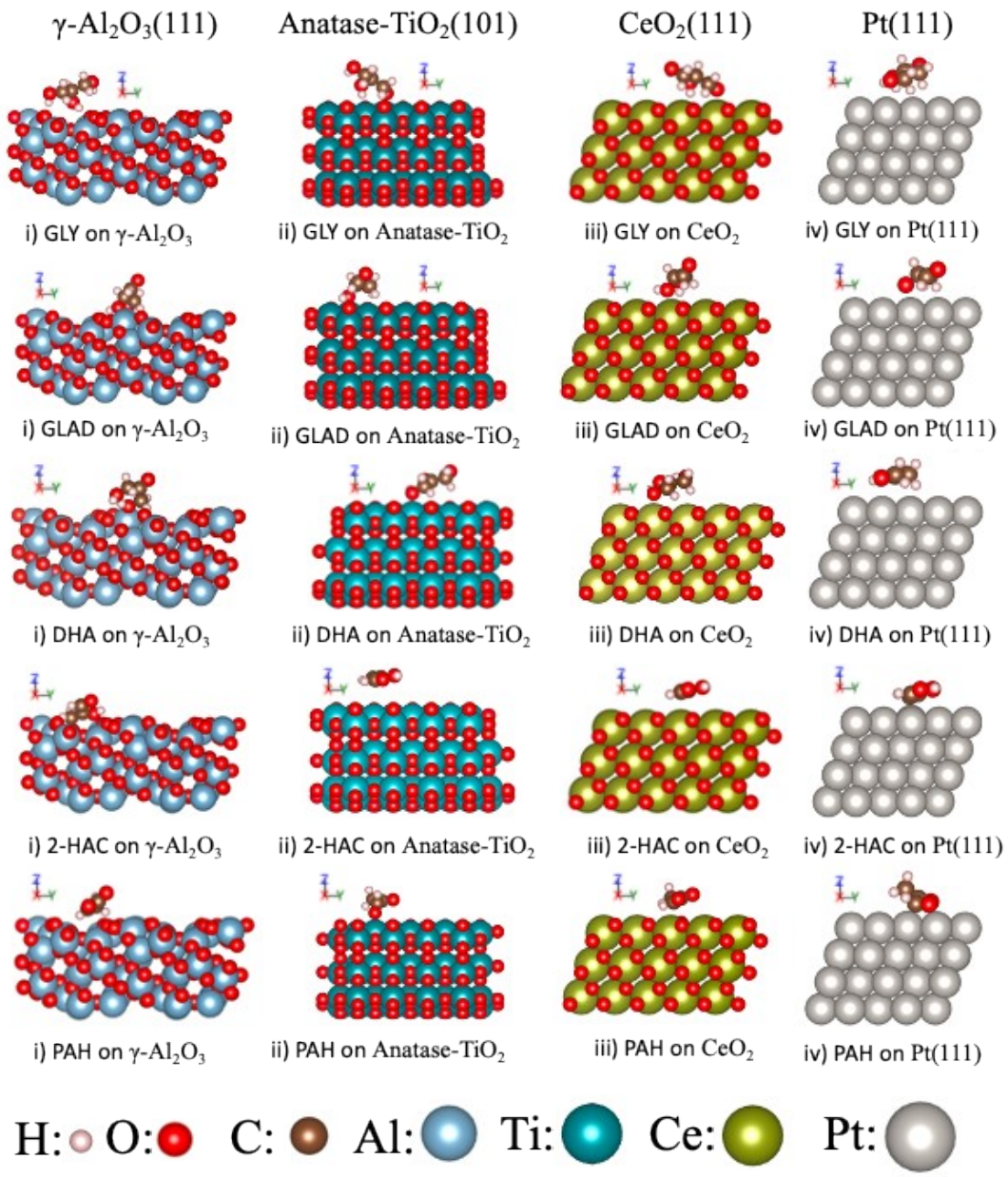

Figure S13. The (Meta-)stable molecules adsorption on different metal/metal oxides, i) γ-Al_2O_3(111), ii) Anatase-TiO_2(101), iii) CeO_2(111) and iv)Pt(111)surface, shown in each row, respectively. In each column, the structures are for different adsorbates, Glycerol (GLY), Glyceraldehyde (GLAD), Dihydroxyacetone (DHA), 2-hydroxyacrylaldehyde (2-HAC) and Pyruvaldehyde (PAH), respectively. As a comparison, the last column is the adsorbates on Pt(111) surface. The correlated free energies are shown in Figure S14.

d. Adsorption energies of reaction intermediates on the studied catalysts

Adsorption Energy, formation energy and Free Energy

Regarding the potential energy by the references of Glycerol$(C_3H_8O_3)$, H_2O and H_2. All the reference states are in gas phase. For different species, the formation energy is:

$$E(C_nH_mO_l) = nE(C) + mE(H) + lE(O)$$

Where $E(C_nH_mO_l)$ is the formation energy of species $C_nH_mO_l$ and n,m,l are stoichiometric number of C,H,O atoms. $E(C)$, $E(H)$ *and* $E(O)$ are the potential

energy of reference atom which are calculated from DFT and reference molecules. Each of the reference molecules were set in the center of a vacuum box whose volume is 15x15x15$Å^3$ and Only the gamma point was considered.
The reference energy of atoms is:

$$E(C) = \frac{1}{3}E(C_3H_8O_3) - E(H_2O) - \frac{3}{2}E(H_2)$$
$$E(O) = E(H_2O) - E(H_2)$$
$$E(H) = \frac{1}{2}E(H_2)$$

For every adsorbate we mentioned in b, the chemical equation of the adsorption process is:

$$C_nH_mO_l(g) + * \rightleftharpoons C_nH_mO_l(*)$$

Where * represents the surface site(s).
We calculated the adsorption energy of a species by:

$$\Delta E_{ads}(C_nH_mO_l) = E_{slab+ads} - E_{slab} - E(C_nH_mO_l)$$

Where $E_{slab+ads}$ is the potential energy of the system (surface + adsorbate), E_{slab} is the potential energy of clean surface, $E(C_nH_mO_l)$ is the formation energy of adsorbate we just mentioned above.

The free energy was calculated by using ASE's thermochemistry module[11]. For reference molecules and stable species we used the Ideal-gas limit. For the adsorbates, we used the Harmonic limit. For the adsorbate frequency, we just calculated the frequency of adsorbate atoms and fixed the surface . The free energy of slab+ads is:

$$G_{Slab+ads} = E_{slab+ads} + ZPE + C_v - TS$$

Where ZPE is the zero-point energy, Cv is the constant volume heat capacity, T is the absolute temperature in K, S is the entropy. From the experimental conditions, the temperature maintained in 60℃. So, we set the temperature as 333K for every calculation.
Considering the free energy of the stable molecules, we use the formation free energy of each molecule to calculate the energy in the free energy diagram. To match the liquid phase, we use vapor pressure of the Glycerol and H_2O to calculate the reference free energy. Hydrogen gas is always in gas phase, so we set the pressure as 1 atm. The reference free energy was calculated by the DFT results and thermodynamic data (tabulated in part g):

$$G_{molecule}(T,P) = E_{molecule} + ZPE + C_v - TS + k_BTln(\frac{P_{vap,molecule}}{P^\circ})$$

Where P° is the standard pressure(1atm), k_B is the Boltzmann constant.
The formation free energy of the intermediates was calculated by the reference states:

$$G(C_nH_mO_l) = nG(C) + mG(H) + lG(O)$$

The free energy of each atom is:

$$G(C) = \frac{1}{3}G(C_3H_8O_3) - G(H_2O) - \frac{3}{2}G(H_2)$$

$$G(O) = G(H_2O) - G(H_2)$$

$$G(H) = \frac{1}{2}G(H_2)$$

In the free energy diagrams (FED), the reference states are each surface and the reference molecules we mentioned above. The Gas phase Glycerol, H_2, H_2O and the clean surface is the starting point of FED which is set to 0. The overall Gibbs free energy of the reaction are calculated by DFT of the gas phase molecule:

$$\Delta G_{reaction} = G_{products} - G_{reactant}$$

In FED, the free energy and Pourbaix diagram plot in each reaction step is:

$$G_{Step} = G_{Slab+ads} - E_{Slab} - G(C_nH_mO_l)$$

Considering the experimental conditions, we use vapor pressure to calculate the free energy of molecules in solution(liquid) phase, as an approximation. In the plot of molecule adsorption (Fig. 4), the adsorption free energy is:

$$\Delta G_{ads,mole}(C_nH_mO_l(l.)) = G_{Slab+ads} - E_{Slab} - G(C_nH_mO_l(l.))$$

Fig. S14 shows the adsorption free energies and formation free energy on the studied catalysts. The related configurations are shown in **Fig. S13**.

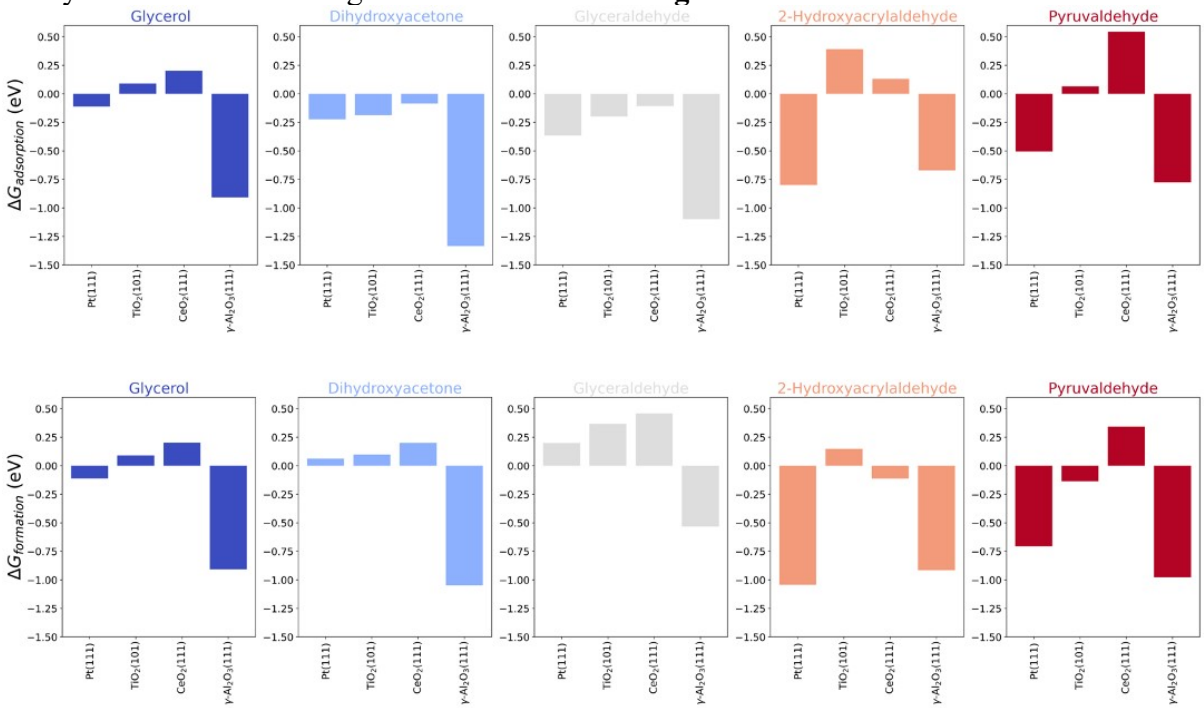

Figure S14. Adsorption free energy (top, referenced to desorbed state) and formation free energy (bottom, referenced to glycerol, H2O and H2). The related adsorption configurations are shown in Figure S13.

e. NH_3-DHA/GLAD adsorption free energies from DFT

We tested the surface acidity from DFT calculations by using the adsorption/desorption energy of ammonia (NH3) as a direct probe, which can be compared to the experimental ammonia TPD results. We sampled different surface sites of NH_3 adsorption and compared their adsorption energy. The most stable adsorption free energy was used in **Fig. S15**.
For Anatase-TiO_2(101), we sampled 2 different Ti-top sites to test the acidity. For the CeO_2(111) and Pt (111), we sampled 1 top site of metal atoms because of the high symmetry of the FCC packed surfaces. For -Al_2O_3, we sampled 5 sites for testing the surface acidity. The surface sites are illustrated in Figure S17. The chosen sites consisted of the unsaturated metal surface atoms, which means the coordination number is less than 6(4 in some cases) analogous to the choice describe in the previous section. The adsorption energies were adopted from the most stable configuration. As shown in **Fig. S15**, the correlation between the adsorption energies of GLAD/DHA and ammonia indicates that the surface acidity affects the binding of the GLAD/DHA. Further, the different trend for GLAD and DHA vs. ammonia indicates the increased preference for surface acidity of DHA over GLAD.

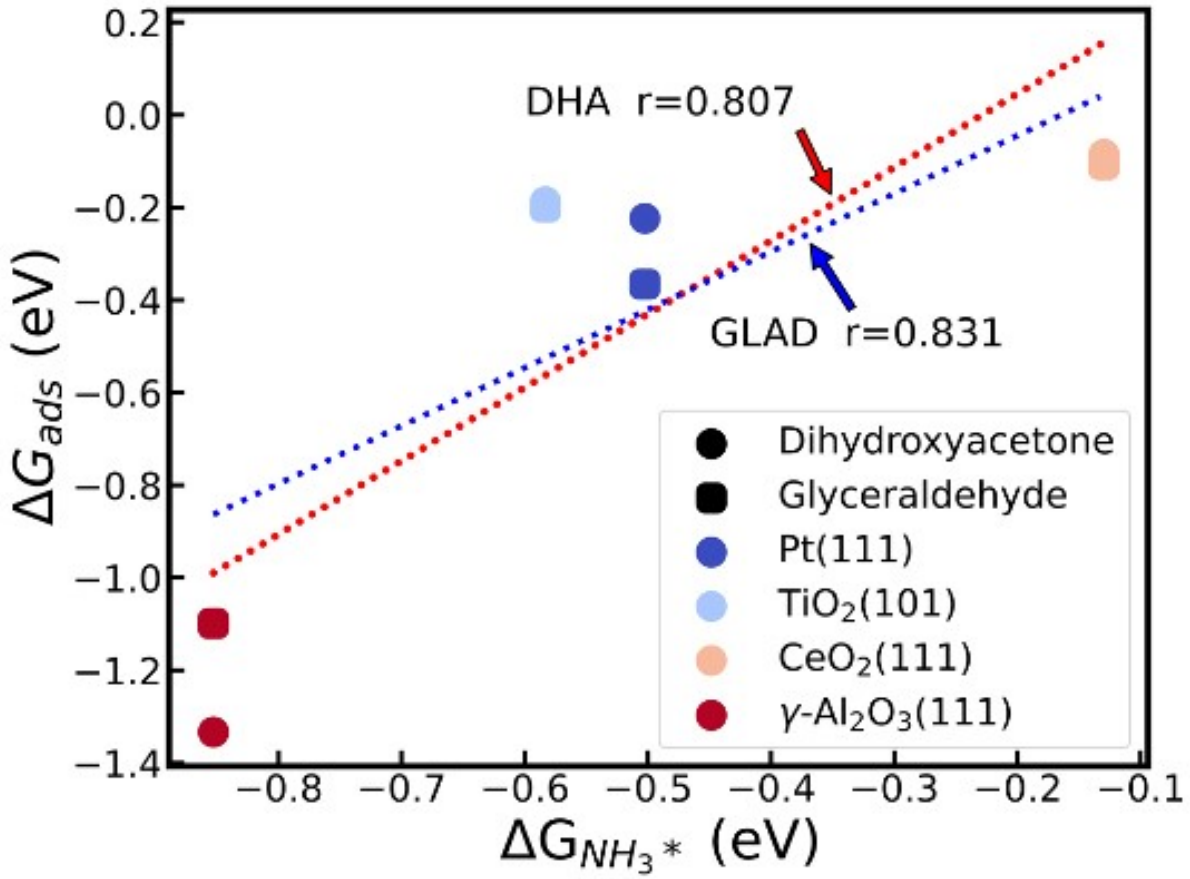

Figure S15. The adsorption free energies of DHA (Circles) and GLAD (Squares) vs. the ammonia adsorption free energy. The dotted lines represent the regression of DHA vs. Ammonia (red) and GLAD vs. Ammonia (blue), respectively. r is the correlation coefficient.

f. Pourbaix Diagram of Metal Oxides

Under electrochemical conditions, the electrode potential will affect the surface phase, especially for metal oxides. In an aqueous interface, the surface will be partially covered with O* or OH* species upon increasing the electrode potential. The two extreme cases are fully metal-terminated and oxygen-terminated surfaces. We calculated the surface Pourbaix Diagrams of the metal oxides using the reduced

(metal-terminated) surfaces as the reference structure. For Anatase-TiO_2(101), we used a 4x2x4 unit cell (bottom 2 layers were frozen) and a kpoint-mesh of 3x6x1. For CeO_2(111), we used a 2x2x3 cell (bottom 2 layers were frozen) a kpoint-mesh of 5x5x1.

For γ-Al_2O_3(111), we used the structure shown in **Fig S12** to calculate the Pourbaix Diagram. For considering the adsorbate-adsorbate interaction, we sampled the traversal combinations of all surface active sites. The active sites consist of the unsaturated metal surface atoms, which means the coordination number is less than 6 (4 in some cases). **Fig. S16** shows the varying symmetrically inequivalent binding sites. The O* and OH* species were adsorbed on the top sites. The reference states for *OH and *O were H_2O and H_2 in gas phase.

For the surface O* formation free energy:

$$*+H_2O(g)\rightarrow O^* + H_2(g) \quad \Delta G^{\circ}_{O*}$$

For the surface OH* formation:

$$*+H_2O(g)\rightarrow OH^* + \frac{1}{2}H_2(g) \quad \Delta G^{\circ}_{OH*}$$

Considering the effect of electrode potential and pH effect, we apply the CHE[10] model, so the formation free energy of OH* or O* can be calculated as:

$$*+H_2O(g)\rightarrow OH^* + H^+ + e^-$$

$$\Delta G_{OH*}(U_{RHE}) = \Delta G^{\circ}_{OH*} + eU_{RHE}$$

$$*+H_2O(g)\rightarrow O^* + 2H^+ + 2e^-$$

$$\Delta G_{O*}(U_{RHE}) = \Delta G^{\circ}_{O*} + 2eU_{RHE}$$

From our results, the most stable surfaces at our experimental conditions (0.5-0.6V vs. RHE) are anatase -TiO_2(101) with the O* species occupying the Ti-bridge sites and CeO_2(111) with O* in the fcc hollow sites. In both cases the metal top sites are uncovered. However, we found γ-Al_2O_3(111) to be covered by a 0.4 ML of OH* (γ-Al_2O_3(111)-OH) at reaction conditions. The *OH coverage strongly influences the binding properties of the surface, as *OH tends to block the acidic sites. However, as we show in Fig. S18, the key intermediates toward lactic acid adsorb even stronger on the surface, replacing OH* at moderate reaction conditions. Thus, we concluded that the surface model of γ-Al_2O_3(111) is more representative than γ-Al_2O_3(111)-OH.

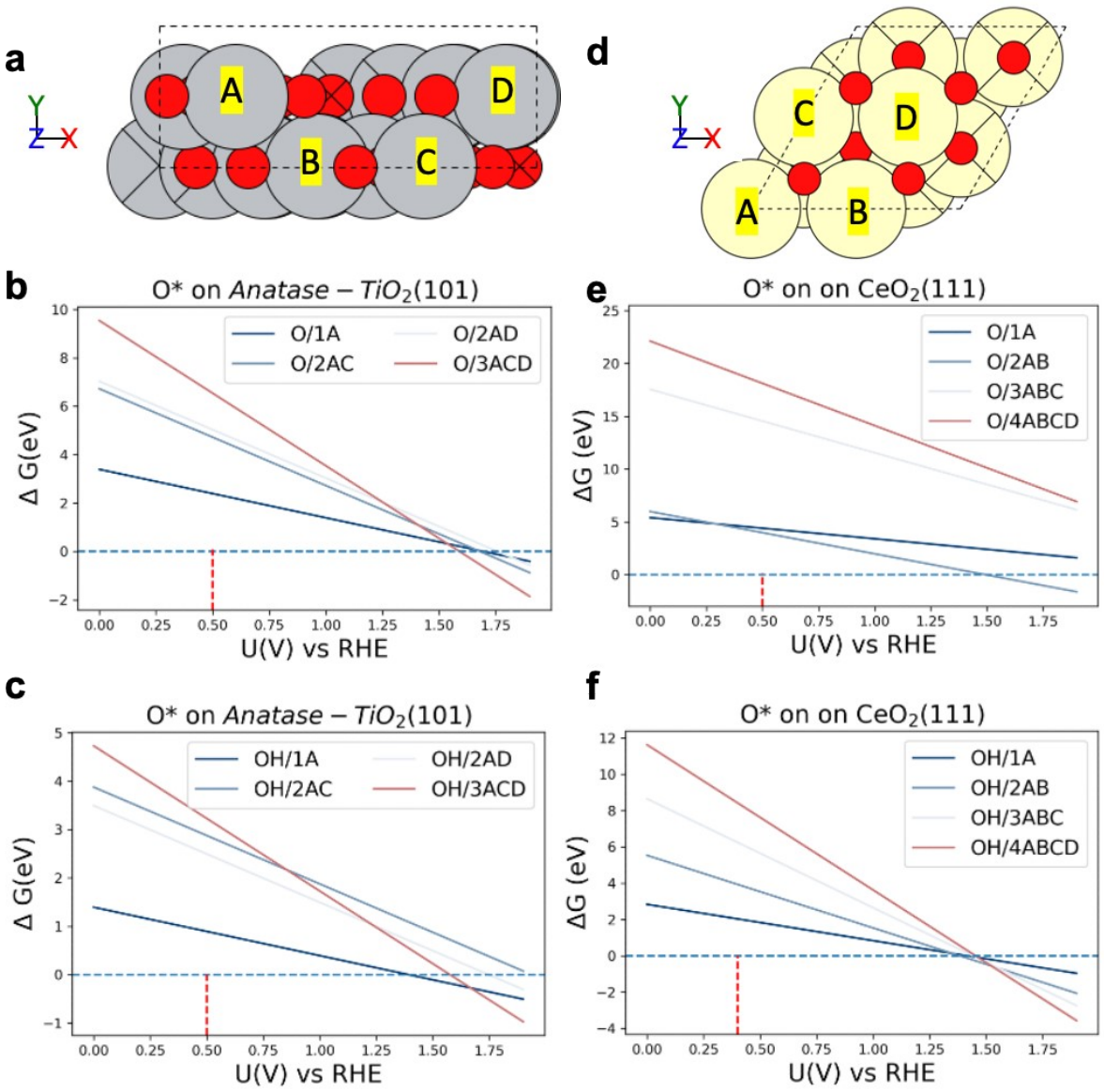

Figure S16 Surface Pourbaix diagrams of Anatase-TiO_2(101) and CeO_2(111). The clean surface structures applied to calculate the Pourbaix diagram are shown in figure S14. The varying binding sites were marked as capital letters. b and c: the Pourbaix diagram of O and OH* adsorption on Anatase-TiO_2(101). e and f: the Pourbaix diagram of O* and OH* adsorption at CeO_2(111). The labels inside panels b,c,e,f correspond to the sampling of the respective sites marked in a,d.*

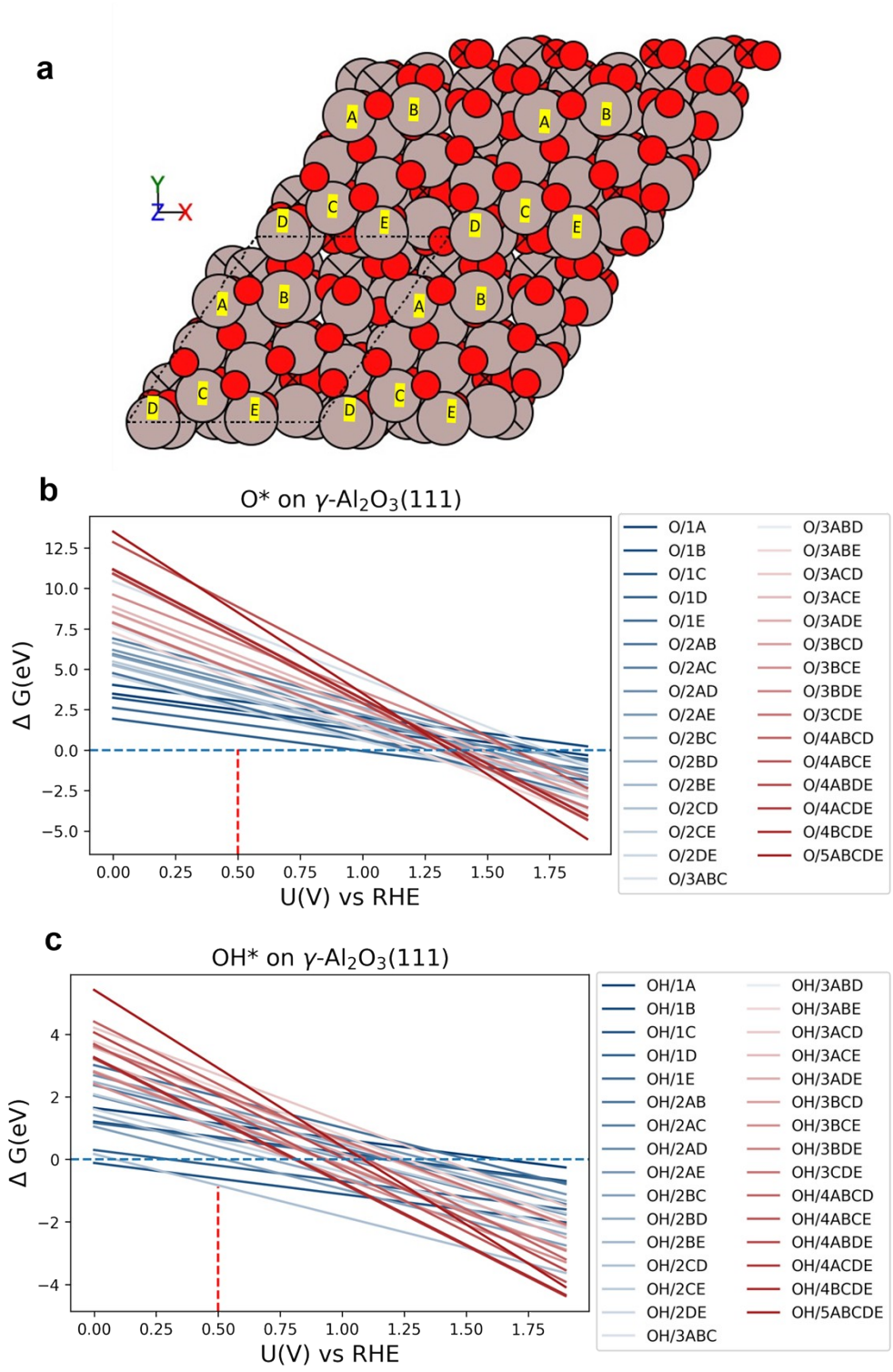

Figure S17 The Pourbaix diagram of γ-Al_2O_3(111), The clean surface structures that applied to calculate the Pourbaix diagram showed in figure S14. The unsaturated sites were marked as the capital letters. In b: the Pourbaix diagram of O adsorption at γ-Al2O3(111). In c: the Pourbaix diagram of OH* adsorption at γ-Al2O3(111). The labels of the panels b,c are the sampling of active sites corresponding to the capital letter marked in a.*

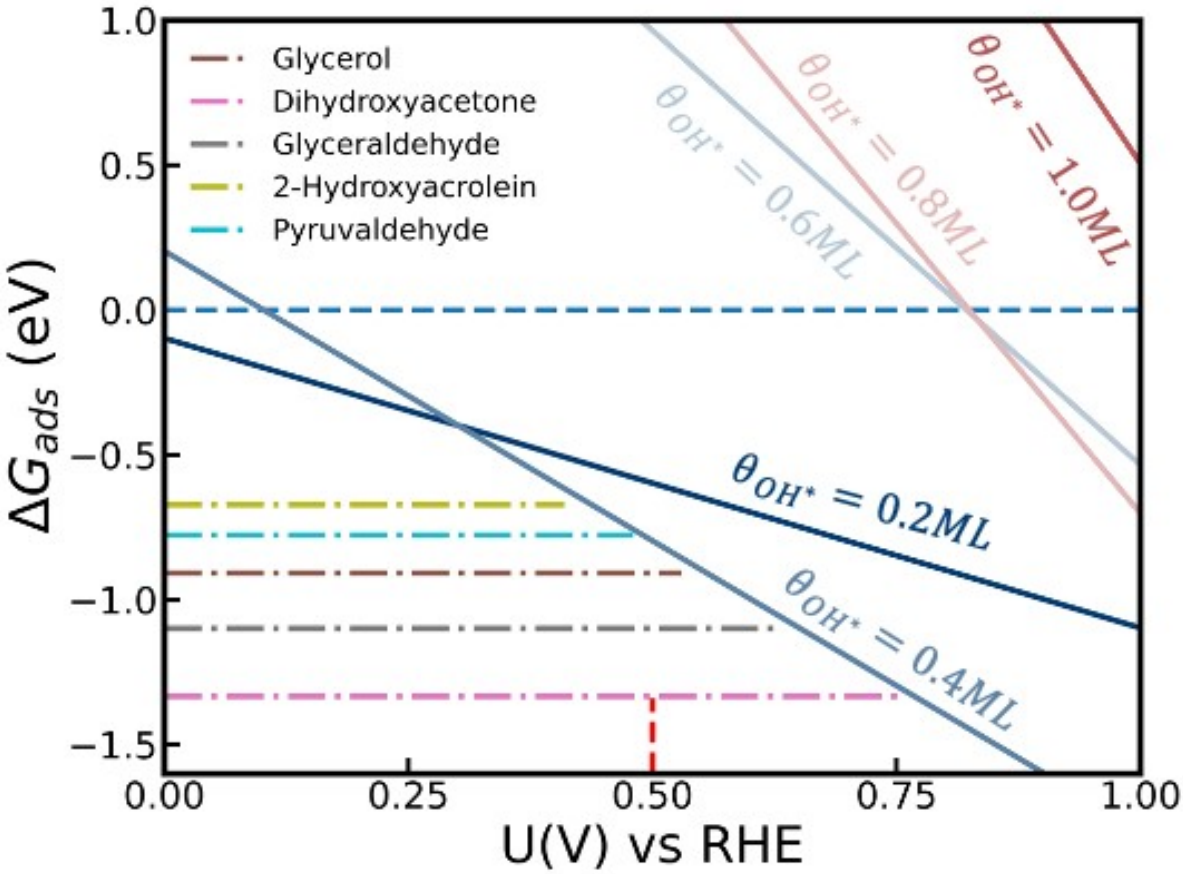

*Figure S18 The Pourbaix diagram of γ-Al_2O_3(111), including the reaction intermediates towards lactic acid. The paralllel dashed-dot lines correspond to the adsorption free energies of the molecules mentioned in the legend. Note that the adsorption energy at the reaction conditions is more negative than the formation energy of *O and *O*

g. Tabulated the Thermodynamic Data

Table S4: Vapor pressure to calculate the free energy of the molecules in this paper .

Molecule	**Equilibrium Vapor Pressure**	**Source**
Glycerol	**25 Pa**	[12]
Glycolic Acid	**1080 Pa**(80 °C)	[13]
Glyceric Acid	**293 Pa**（25 °C）	ChemSrc
Formic Acid	**5333 Pa**	[14]
Tartronic Acid	**0.00025 Pa**	[15]
Lactic Acid	**ca. 10 Pa**	lambic.info
H_2O	3282 Pa	[14]
H_2(g)	101325Pa	1 atm
NH_3(g)	101325Pa	1 atm

Table S5: The point group and symmetry number of molecules that is applied to calculate the thermal properties of adsorption structures[16]

Molecules	**Point group**	**Symetry Number**
NH_3	**C_{3v}**	**3**

Glycerol	**C_s**	**1**
Dihydroxyacetone	**C_{2h}**	**2**
Glyceraldehyde	**C_1**	**1**
2-Hydroxyacrolein	**C_s**	**1**
Pyruvaldehyde	**C_s**	**1**
Lactic Acid	**C_1**	**1**
Glyceric Acid	**C_1**	**1**
Tartronic Acid	**C_s**	**1**
Glycolic Acid	**C_s**	**1**
Formic Acid	**C_s**	**1**
H_2O	**C_{2v}**	**2**
H_2	**$D^{\infty}{}_h$**	**2**

6. Reference

1 Gu, J., Wang, J. & Leszczynski, J. Structure and Energetics of (111) Surface of γ-Al2O3: Insights from DFT Including Periodic Boundary Approach. *ACS Omega* **3**, 1881-1888 (2018). https://doi.org:10.1021/acsomega.7b01921

2 Kresse, G. & Furthmüller, J. Efficient iterative schemes for ab initio total-energy calculations using a plane-wave basis set. *Physical Review B* **54**, 11169-11186 (1996). https://doi.org:10.1103/PhysRevB.54.11169

3 Kresse, G. & Joubert, D. From ultrasoft pseudopotentials to the projector augmented-wave method. *Physical Review B* **59**, 1758-1775 (1999). https://doi.org:10.1103/PhysRevB.59.1758

4 Hammer, B., Hansen, L. B. & Nørskov, J. K. Improved adsorption energetics within density-functional theory using revised Perdew-Burke-Ernzerhof functionals. *Physical Review B* **59**, 7413-7421 (1999). https://doi.org:10.1103/PhysRevB.59.7413

5 Grimme, S., Antony, J., Ehrlich, S. & Krieg, H. A consistent and accurate ab initio parametrization of density functional dispersion correction (DFT-D) for the 94 elements H-Pu. *The Journal of Chemical Physics* **132**, 154104 (2010). https://doi.org:10.1063/1.3382344

6 Tait, S. L., Dohnálek, Z., Campbell, C. T. & Kay, B. D. n-alkanes on MgO(100). I. Coverage-dependent desorption kinetics of n-butane. *The Journal of Chemical Physics* **122**, 164707 (2005). https://doi.org:10.1063/1.1883629

7 Monkhorst, H. J. & Pack, J. D. Special points for Brillouin-zone integrations. *Physical Review B* **13**, 5188-5192 (1976). https://doi.org:10.1103/PhysRevB.13.5188

8 Hu, Z. & Metiu, H. Choice of *U* for DFT+*U* Calculations for Titanium Oxides. *J. Phys. Chem. C* **115**, 13, 5841–5845 (2011). https://doi/abs/10.1021/jp111350u

9 Cramer, C. J. & Bickelhaupt, F. Essentials of computational chemistry. *ANGEWANDTE CHEMIE-INTERNATIONAL EDITION IN ENGLISH-* **42**, 381-381 (2003).

10 Nørskov, J. K. *et al.* Origin of the Overpotential for Oxygen Reduction at a Fuel-Cell Cathode. *The Journal of Physical Chemistry B* **108**, 17886-17892 (2004). https://doi.org:10.1021/jp047349j

11 Hjorth Larsen, A. *et al.* The atomic simulation environment—a Python library for working with atoms. *Journal of Physics: Condensed Matter* **29**, 273002 (2017). https://doi.org:10.1088/1361-648x/aa680e

12 Cammenga, H. K., Schulze, F. W. & Theuerl, W. Vapor pressure and evaporation coefficient of glycerol. *Journal of Chemical and Engineering Data* **22**, 131-134 (1977).

13 Daubert T, E. Physical and Thermodynamic Properties of Pure Chemicals : Data Compilation. *Design Institute for Physacal Property Data(DIPPR)* (1989).

14 Haynes, W. M., Lide, D. R. & Bruno, T. J. *CRC handbook of chemistry and physics*. (CRC press, 2016).

15 Booth, A. M. *et al.* Solid state and sub-cooled liquid vapour pressures of substituted dicarboxylic acids using Knudsen Effusion Mass Spectrometry (KEMS) and Differential Scanning Calorimetry. *Atmos. Chem. Phys.* **10**, 4879-4892 (2010). https://doi.org:10.5194/acp-10-4879-2010

16 Cramer, C. J. *Essentials of computational chemistry: theories and models*. (John Wiley & Sons, 2013).